Journal of the European Ceramic Society 20 (2000) 1121–1128

Finite element modelling of cold isostatic pressing

R.J. Henderson[a], H.W. Chandler[a,*], A.R. Akisanya[a], H. Barber[a], B. Moriarty[b]

[a]*Department of Engineering, Fraser Noble Building, University of Aberdeen, Aberdeen AB24 3UE, UK*
[b]*Vesuvius UK, Newmilns, Ayrshire KA16 9AG, UK*

Received 28 June 1999; accepted 5 October 1999

Abstract

Cold isostatic compaction, where a shaped rubber bag is filled with powder, sealed and then subjected to high all-round pressure to produce a compacted green component, is a common processing route for ceramic components. The key to isostatic pressing is the design of the rubber bag which is in general both different in size and shape from the green body. This paper presents: the results of experiments to measure the powder and elastomer properties; finite element simulations of cold isostatic pressing; and comparisions between the two. The finite element simulations use an elasto-plastic, volume hardening plasticity model for the compacting powder and a finite deformation hyperelastic model for the rubber. The simulations give excellent agreement with experimental results for the pressed component shape, and highlight the importance of including the elastomeric bag within the simulations.

Keywords: Cold isostatic pressing; Finite element modelling; Pressing; Refractories

1. Introduction

Isostatic pressing is one method of producing high quality green ceramic components. It has the advantages of producing products with close to uniform density from relatively inexpensive tooling[1] with the potential for rapid response to product changes. It is particularly suited to the manufacture of shaped tubes with a high length-to-diameter ratio, for example: ladle shrouds; subentry nozzles; and subentry shrouds.

The key to successful isostatic pressing is the design of the elastomeric bag in which the powder is pressed.[2] This design process is more complicated than might be expected as the bag is in general both different in shape and size from the final green body. In current industrial practice, the elastomeric bag shape is chosen either by trial and error, with the aid of simple compaction calculations, or based upon past experience. One possible tool to help improve the bag design process and reduce the number of increasing stressful trial and error cycles, is the finite element simulation of the pressing process.

Although many authors have, with some success, utilised the finite element method to model the die compaction of ceramic powders,[3,4] the modelling of isostatic pressing is not so widely reported in the literature. In particular, few authors[5] have considered the change in shape of the elastomeric bag during the initial stages of compaction.[6] Whilst ignoring the elastomeric bag is a reasonable assumption for simple geometries,[7] for more complex shapes the inclusion of the bag in the analysis is essential for accurate prediction of distortion.

This paper consolidates and extends the work described in Sugita et al.[5] by including the deformation of the bag in the finite element modelling of powders with relatively rigid inserts. Some of the complexities of the finite element modelling include finite deformation, nonlinear material behaviour and the concurrent use of compressible plasticity and incompressible elasticity. The methods developed are rigorously validated and have been used to predict the green geometries of two refractory components. The predictions will be shown to be in good agreement with experimental results.

2. Constitutive model

Whilst the constitutive behaviour of many engineering materials is understood, and generally accepted constitutive models exist, this is not the case for powder

* Corresponding author.

0955-2219/00/$ - see front matter
PII: S0955-2219(99)00280-0

materials. The most notable feature of powder materials is their ability to undergo permanent volume reduction as a result of hydrostatic pressure. This volume reduction can be enhanced by the application of shear. Therefore, any model which accurately describes the deformation of a powder, under non-hydrostatic loading, should include this shear-volume coupling. To complicate the modelling further, powder materials can undergo deformation by a number of mechanisms:

1. Rearrangement of particles. This can lead to either an increase (dilation)[8] or decrease in the bulk volume. This mechanism occurs in general when the applied hydrostatic stress is low compared to the shear stresses, for example during vibration of loose filled powders, or at the onset of isostatic loading.
2. Contact patch deformation between the grains. This mechanism occurs when the applied stresses are high enough to produce yielding of the agglomerated material at the contact patches.
3. Fracture of the ceramic grains. Whilst this was originally thought to be present only at high applied pressures, recent work has shown that this deformation mechanism can occur at relatively low pressures.[9]

Many models have been developed[10–15] to describe the constitutive behaviour of powders during deformation. These models can simulate many of the features of powder deformation (for example shear-pressure coupling, dilation and anisotropy). However, these models have been developed for particular loadings and at present no model appears to fully describe the deformation of powders for truly general loading. In order to simulate isostatic pressing it is, therefore, necessary to select a constitutive model, which combines the required material features and numerically stability.

As powder particles can range from spherical metal balls to coarse angular alumina grains it is important to consider the microstructure of the powder in order to determine the deformation mechanism. In this report we simulate the deformation of a rounded agglomerate consisting of large alumina grains coated in flake graphite and a organic binder. The microstructure of the powder after compaction does not indicate any fracture of the large alumina grains and therefore it can be concluded that particle rearrangement and contact patch deformation are the primary deformation mechanisms.

During isostatic compaction of casting conduits, the shear stresses are, in general, low compared to the pressure and, therefore, after initial rearrangement, the deformation is controlled by contact patch deformation between the agglomerates. The loading is also in general proportional, that is the ratios of the components of stress remains close to constant during the pressing process. This is illustrated in Fig. 1.

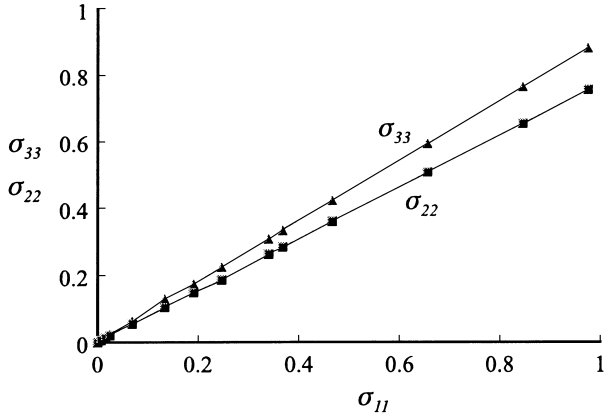

Fig. 1. Illustration of near proportional loading seen in finite element simulations of isostatic compaction of a typical continuous casting component.

Experimental triaxial tests on ceramic powders have shown that for near-hydrostatic loading the apparent yield surface in principle stress space can be approximated by an elliptical yield surface[10] (Fig. 2). Therefore, an elasto-plastic constitutive model with an elliptical yield surface has been utilised. This has been implemented in a subroutine within the commercially available finite element code ABAQUS.

In order to implement any constitutive model within an implicit finite element code it is necessary to obtain the elasto-plastic stiffness matrix ($\mathbf{K}_{ep}$) which relates the stress increment $\dot{\boldsymbol{\sigma}}$ to the strain increment $\dot{\mathbf{e}}$.

$$\dot{\boldsymbol{\sigma}} = \mathbf{K}_{ep}\dot{\mathbf{e}} \tag{1}$$

One method of obtaining ($\mathbf{K}_{ep}$) for an elasto-plastic constitutive model is described below. For clarity, column vectors are denoted in bold lowercase and matrices in bold uppercase. The yield function (ψ) depends upon the stress ($\boldsymbol{\sigma}$) within the material and the state of hardening of the material denoted by $\mathbf{h}$. For volumetric

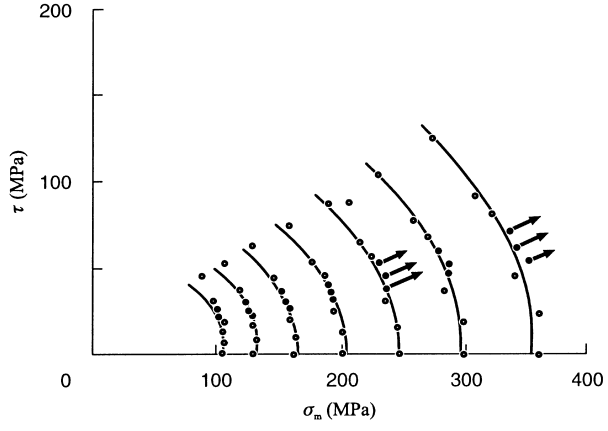

Fig. 2. The results obtained by Shima and Mimura for ceramic powders. This shows that the approximation of an elliptical yield surface is valid close to the hydrostatic axis.

hardening $\mathbf{h}$ is a scalar value. The approach given here, however, allows extension to include other hardening parameters with only a small increase in complexity. The stress state within the body at yield is given by $\psi(\boldsymbol{\sigma}, \mathbf{h}) = 0$. To maintain this during deformation

$$\left(\frac{\partial \psi}{\partial \boldsymbol{\sigma}}\right)^T \dot{\boldsymbol{\sigma}} + \left(\frac{\partial \psi}{\partial \mathbf{h}}\right)^T \dot{\mathbf{h}} = 0, \tag{2}$$

where superscript T denotes the transpose of the matrix, $\dot{\boldsymbol{\sigma}}$ is the stress increment and $\dot{\mathbf{h}}$ is the change in hardening through the increment. $\dot{\mathbf{h}}$ can be expressed in terms of the plastic strain $\dot{\mathbf{e}}^p$

$$\dot{\mathbf{h}} = \left(\frac{\partial \mathbf{h}}{\partial \mathbf{e}}\right)^T \dot{\mathbf{e}}^p. \tag{3}$$

The flow vectors determine the direction of the strain increment and if it is assumed that these are normal to the yield surface then the plastic strain can be written as

$$\dot{\mathbf{e}}^p = \dot{\lambda} \frac{\partial \psi}{\partial \boldsymbol{\sigma}}, \tag{4}$$

where λ is a positive number which varys with position. Some simple rearrangement of (2)–(4) gives the plastic strain increment

$$\dot{\mathbf{e}}^p = \frac{\dfrac{\partial \psi}{\partial \boldsymbol{\sigma}}\left(\dfrac{\partial \psi}{\partial \boldsymbol{\sigma}}\right)^T}{\left(\dfrac{\partial \psi}{\partial \mathbf{h}}\right)^T \left(\dfrac{\partial \mathbf{h}}{\partial \mathbf{e}}\right)^T \dfrac{\partial \psi}{\partial \boldsymbol{\sigma}}} \dot{\boldsymbol{\sigma}} = \mathbf{P}\dot{\boldsymbol{\sigma}}. \tag{5}$$

As $\mathbf{P}$ is formed from the dyadic product of two vectors $\left(\frac{\partial \psi}{\partial \boldsymbol{\sigma}}\left(\frac{\partial \psi}{\partial \boldsymbol{\sigma}}\right)^T\right)$ it is singular and cannot be inverted directly. It is, therefore, necessary to introduce the elastic strains $\mathbf{e}^e$ and elastic stiffness matrix $\mathbf{K}_e$. The total strain is the sum of the plastic strain and the elastic strain

$$\dot{\mathbf{e}} = \dot{\mathbf{e}}^e + \dot{\mathbf{e}}^p \tag{6}$$

and therefore

$$\dot{\mathbf{e}} = (\mathbf{K}_e^{-1} + \mathbf{P})\dot{\boldsymbol{\sigma}}. \tag{7}$$

It is now possible to invert Eq. (7) using the Sherman-Morrison formula[16] to give

$$\dot{\boldsymbol{\sigma}} = \left(\mathbf{K}_e - \frac{\mathbf{K}_e \mathbf{P} \mathbf{K}_e}{1 + \mathrm{tr}(\mathbf{P}\mathbf{K}_e)}\right)\dot{\mathbf{e}}. \tag{8}$$

This elasto-plastic stiffness matrix is true for any elasto-plastic constitutive model with associated flow and strain hardening.

A particular example of an elliptical yield surface has the yield function

$$\psi = \frac{s_{ij}s_{ij}}{k^2} + \frac{\sigma^2}{l^2} - 1 = 0, \tag{9}$$

where $\sigma = \sigma_{11} + \sigma_{22} + \sigma_{33}$. s_{ij} is the deviatoric stress

$$s_{ij} = \sigma_{ij} - \frac{1}{3}\sigma\delta_{ij} \tag{10}$$

where δ_{ij} is the Kronecker delta. In Eq. (9) k and l are adjustable parameters which depend upon the volume of the material. Their ratio determines the ellipticity of the yield surface. Previous work on ceramic powders has shown that this is constant during deformation for many powders.[17]

In order to simulate the compaction process there are, therefore, two key material properties; the hydrostatic pressure-volume strain behaviour which gives the evolution of l with deformation; and the ratio k/l which can be determined from the lateral stress ratio in uniaxial die pressing.[17]

3. Determination of material properties

3.1. Ceramic powder

3.1.1. Pressure-volume relationship

The pressure-volume strain behaviour [i.e. l as a function of density in Eq. (9)] of the ceramic powder was measured using an instrumented isostatic press. Refractory powder (agglomerated graphite, alumina and binder) was placed in an elastomeric bag (100 mm long, 50 mm diameter) and lightly vibrated. The bag was then sealed by a steel closure (Fig. 3) and subjected to a hydrostatic pressure. Due to the presence of the steel closure the compaction is not truly isostatic. Finite element modelling of the test piece, however, shows that in the bulk of the specimen the stress state is very close to isostatic.

Typical results for the stress–strain behaviour are shown in Fig. 4. Similar to many ceramic powders,[18] the material exhibits an almost linear low pressure hardening region where the majority of the compaction occurs. The material then hardens rapidly. The small differences between specimens were attributed to variations in the initial fill density.

3.1.2. Ratio of k/l

The ellipticity of the yield surface can be inferred by using an instrumented die press as described in Song and Chandler.[17] A similar apparatus to that used in Song and Chandler[17] was built (Fig. 5) with strain gauges mounted axially and circumferentially on the outer surface of a thin cylinder allowing measurement of the stresses transmitted to the die. The powder was placed in the die and compressed on a universal testing machine (Instron 1185) at a nominal axial strain rate of

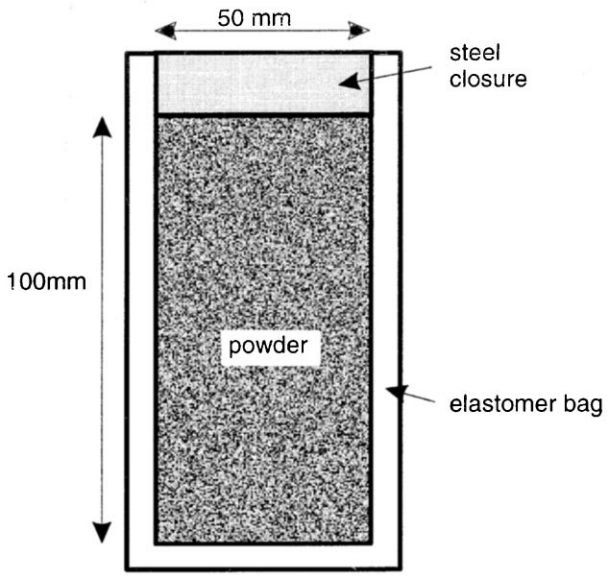

Fig. 3. The tooling used to measure the hydrostatic pressure-volume strain behaviour of the material.

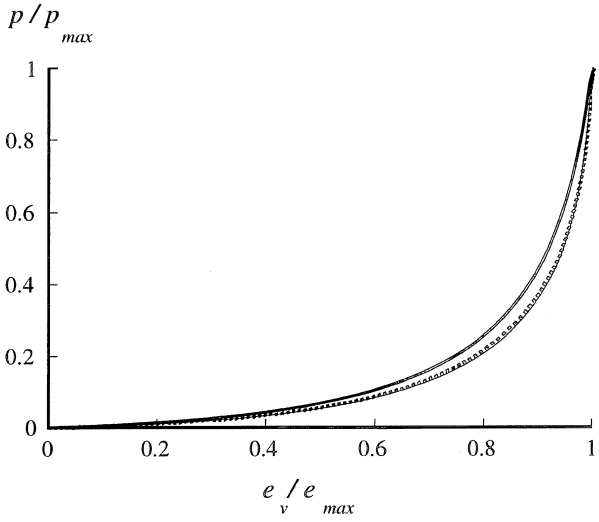

Fig. 4. The pressure-nominal volume strain behaviour of the ceramic powder for three separate samples. Any differences between specimens were attributed to the initial fill density. The data has been normalised with respect to the maximum strain (e_{max}) and the maximum pressure (p_{max}).

0.02 s^{-1}. During the test the strains in the cylinder, the applied load and displacement were continually monitored.

In Song and Chandler[17] the data obtained from this test was interpreted by the solution of an integral equation with the Green's function for the axisymmetric loading of a tube as the kernel. We have, however, interpreted the data using finite element simulations of the die press. The mesh is shown in Fig. 6. The ellipticity of the yield surface and the coefficient of friction between the powder and die wall were varied until good agreement was obtained between the experimental and

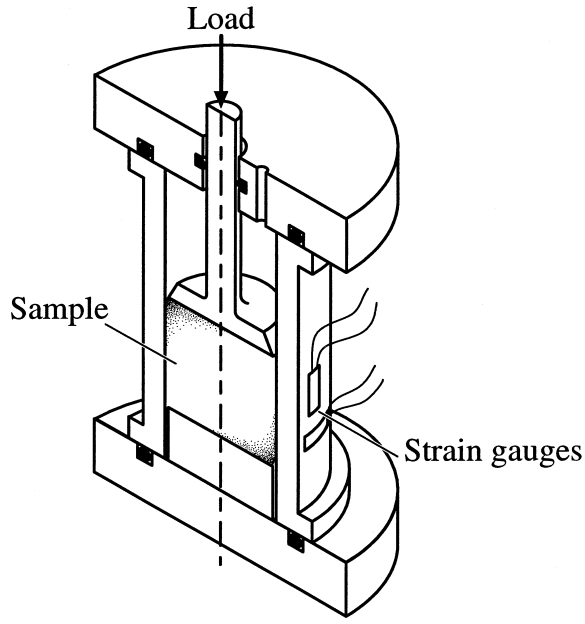

Fig. 5. Schematic of the instrumented die press, showing the strain gauges which measure the hoop and axial strain induced in the die during pressing.

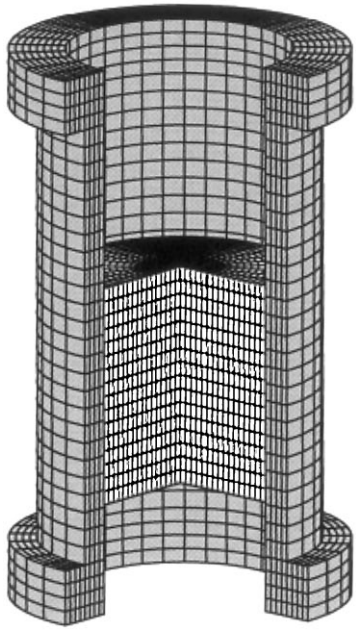

Fig. 6. Example finite element mesh of the die press used to calibrate the material model.

finite element results for the strains on the outer surface of the die (Fig. 7).

3.2. Elastomer properties

A number of authors who have used the finite element method to model isostatic pressing have not included the elastomeric bag. However, in the initial stages of

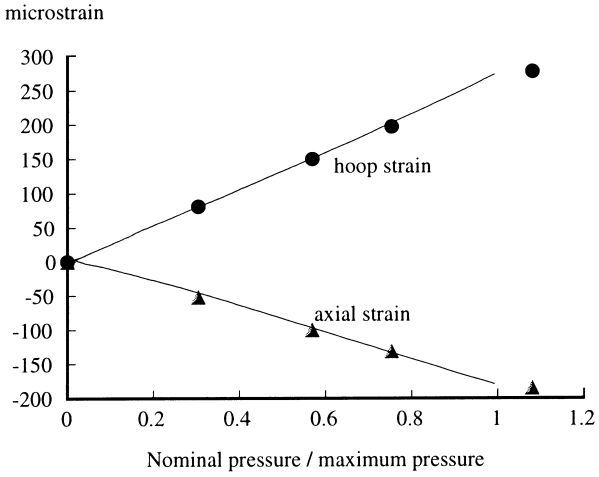

Fig. 7. Comparison of the finite element predictions (points) and experimental results (lines) for the strains induced in the die wall during die compaction.

compaction, where the elastomer is stiffer than the powder the bag plays an important role and is one source of distortion in the final component. It is, therefore, necessary to determine the properties of the elastomeric bag.

Using the instrumented isostatic press, described above, the hydrostatic stress–volumetric strain behaviour of the elastomer was measured. The material was also tested in uniaxial tension on a Houndsfield 10KS testing machine. The uniaxial strain in the sample was measured using a Houndsfield 500L non-contacting laser extensometer. As the strains induced in the elastomer bag are relatively large (up to 20%) the elastomer bag was modelled using a Mooney–Rivlin finite deformation formulation[19] with the material properties obtained from the mechanical testing.

4. Finite element modelling

If the constitutive behaviour of the powder and elastomer are known then it is possible to numerically model the deformation process. In our simulations the constitutive model described in Section 2 has been implemented within a user defined subroutine within the commercial finite element code ABAQUS. Two geometries have been chosen to illustrate the modelling, an axisymmetric ladle shroud (Fig. 8), and an initially square cross-section (Fig. 10).

4.1. Axisymmetric component

Many continuous casting components have rotational symmetry and therefore, can be modelled using axisymmetric finite elements. The component was meshed using the FEMSYS[20] software package and the analysis was performed using the implicit finite element code ABAQUS Standard.[21] As we are primarily interested in the powder displacements it is not necessary to excessively refine the mesh. Throughout the model quadratic (6 noded triangles and 8 noded quadrilateral) elements with full integration (9 Gauss points per quadrilateral and 3 Gauss points per triangle) were used. In order to model the incompressibility of the elastomer bag hybrid finite elements with constant pressure were used in this region.

In order to model the interaction of the bag with the powder, it was assumed that there was no slip at the bag–powder interface. This is a reasonable assumption as the bag material is soft compared to the alumina containing powder agglomerates which indent the bag. In addition, examination of an elastomeric bag after it has been used to press many components indicates very little wear. The interaction of the powder with the metal insert was modelled by allowing the powder to slide on the vertical section of the mandrel and by holding it fixed on the horizontal end caps.

As the problem has both geometrical and material non-linearities the pressure was applied in a series of small increments, a solution being obtained at the end of each load increment. The shape of the final green component as simulated by the finite element model is shown in Fig. 9.

4.2. Plane strain model

If a component does not have any rotational symmetry it is necessary to carry out a fully three-dimensional analysis. This is expensive, not only in the time required for meshing the component, but also computationally. It is, therefore, useful to consider methods for simplifying the modelling of these complex components. During pressing many continuous casting pipes have a steel mandrel through most of the length of the component. Where a steel mandrel is present the strain-state perpendicular to the mandrel is very close to plane strain conditions. For example the axisymmetric model described above shows that the strains parallel to the mandrel are an order of magnitude lower than those perpendicular to the mandrel. This approximation, therefore, allows a cross-section through a component to be modelled using two-dimensional plane strain elements. By assembling a number of cross-sections a good approximation of the component geometry can be obtained. It should be noted that this method is only valid if the cross-section is changing shape and size slowly along the length of the component. This approach was used to model the, initially square, cross-section.

In this case the mandrel was modelled by finite elements, and no slip between the powder and mandrel was permitted. It is also only necessary to model one quarter of the component because of symmetry. The interaction of the powder with the elastomer bag was

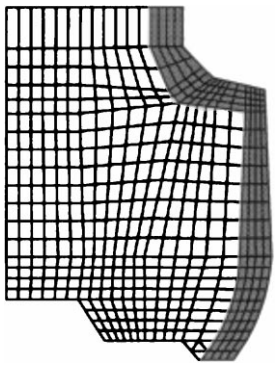

Fig. 8. Typical finite element mesh used in the flange section of the axisymmetric ladle shroud. The elastomer bag is represented by the shaded region.

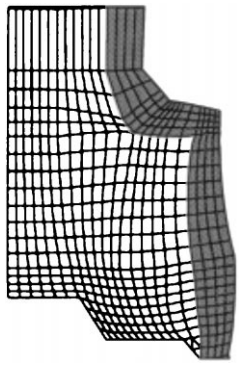

Fig. 9. Shape predicted by the finite element analysis for the flange section. Note that not only have the sizes of the component changed, but also the shape.

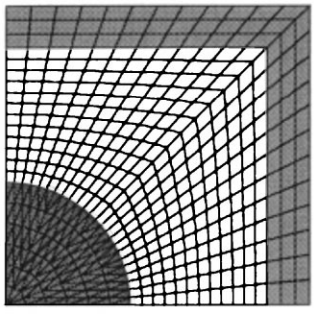

Fig. 10. Initial mesh for the square cross-section. It is only necessary to model one quarter due to the symmetry of the component. Again the back is shown by the shaded region and the mandrel by the darkest region.

treated the same as in the axisymmetric problem. The result of the simultaion is shown in Fig. 11.

4.3. Comparison of geometries

To test the accuracy of the finite element predictions several components were manufactured and the dimensions of the component after compaction were compared with the finite element predictions. The components were

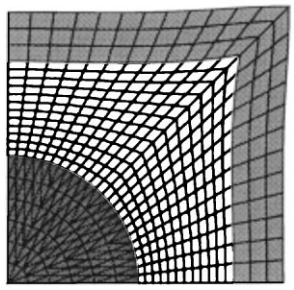

Fig. 11. Shape predicted by the finite element analysis for the square component modelled in plane strain.

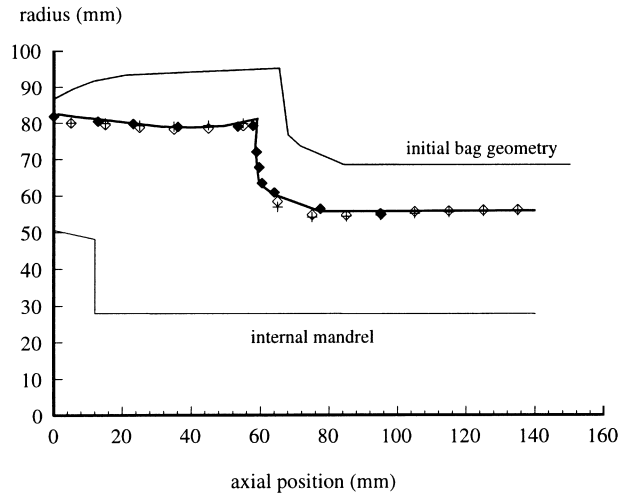

Fig. 12. Comparison of predicted results and those obtained from experiments for the flange section. The experimental results are denoted by points and the finite element predictions are denoted by the line. The initial shape of the elastomeric bag has also been included to give an idea of the amount of deformation.

measured using a three dimensional coordinate measuring machine (Rank–Taylor–Hobson Tallycheck III). In the case of the axisymmetric component the radius was taken as the average of eight measurements around the circumference.

The results obtained for the two geometries are compared with the finite element results in Figs. 12 and 13. Both geometries show excellent agreement between the experimental and numerical results, with a typical radial error of less than 1.5 mm on a component of radial dimension 60 mm.

4.4. Effect of the elastomeric bag

In order to highlight the effect of the elastomeric bag has on the distortion of the component during pressing a ladle shroud flange section was modelled without including the elastomeric bag. The pressure was, therefore, applied directly to the powder. The deformed shape is shown in Fig. 14. Whist the gross shape gives good agreement with the measured component there are

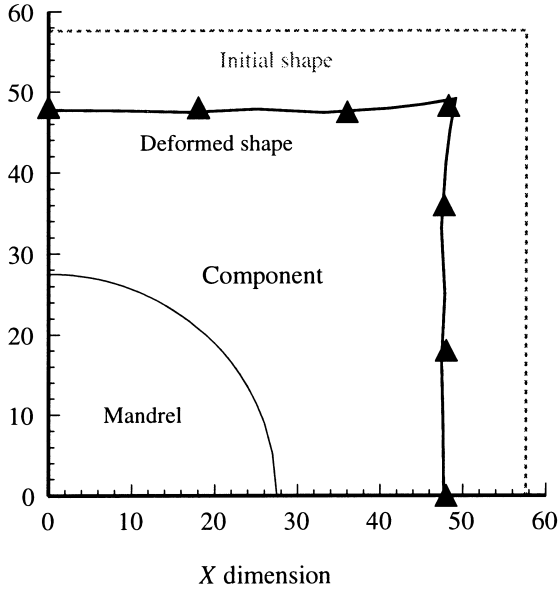

Fig. 13. Comparison of predicted results and those obtained from experiments for the square cross-section. The finite element results are shown by the line, and the experimental results by the points.

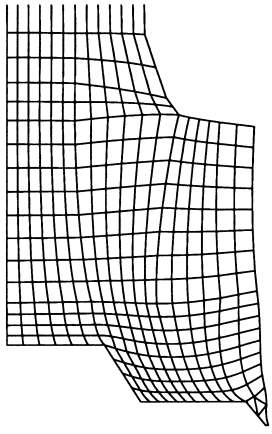

Fig. 14. Finite element prediction of the deformation, when the elastomer bag is omitted from the model. The gross deformation is of the right order. However, there is no flattening of the flange section (for composition see Fig. 8).

significant differences in the horizontal section of the flange which has not flattened as observed in experiments. This illustrates the importance of including the elastomeric properties of the bag in the finite element simulations.

5. Conclusions

1. Finite element modelling, with suitable material models, can be used to accurately predict the green form of components manufactured by cold isostatic pressing.
2. The finite element modelling indicates the importance of including the elastomeric bag within the predictions, as the elastomeric bag is one source of distortion within the pressing process.
3. For complex three-dimensional components, where a steel mandrel is utilised, reasonable results are obtained by modelling cross-sections through the geometry in plane strain.

Acknowledgements

The authors would like to thank EPSRC and Vesuvius UK for financial assistance and S.A. Nixon for assistance with the diagrams.

References

1. Morris, K. J., Cold isostatic pressing for forming ceramics. In *Encyclopedia of Materials Science and Engineering, Vol. 1*, ed. H. B. Bever. Pergamon Press, Oxford, 1986, pp. 707–711.
2. Morris, K.J., Tooling for cold isostatic pressing. In *Isostatic Pressing Technology*, ed. P.J. James. Applied Science Publications, 1983.
3. Briscoe, B, Aydin, I. and Sanliturk, K. Y., The internal form of compacted ceramic components: a comparison of finite element modelling with experiment. *Powder Technology*, 1996, **89**, 239–254.
4. Zipse, H., Finite-element simulation of the die pressing and sintering of a ceramic component. *J. Eur. Ceram. Soc.*, 1997, **17**, 1707–1713.
5. Sugita, T., Sugita, S., Hamanaka, J., Nakatsuka, M. and Koga, S., Mechanical behaviour of the ceramic granule in cold isostatic pressing. *JSME International Edition*, 1992, **35**, 470–474.
6. Chandler, H. W. and Song, J. H., Mathematical modelling of isostatic pressing. *Br. Ceram. Trans. J.*, 1989, **88**, 167–172.
7. Takehana, N., Nakagawa, T., Nakayama, K. and Naoi, T., Numerical analysis of powder compaction during isostatic pressing. *Int. Conf. Powder. Metall*, 1990, **3**, 148–151.
8. Reynolds, O., On the dilatancy of media composed of rigid particles in contact with experimental observations. *Phil. Mag.* (Series 5), 1885, **20**, 469–481.
9. McDowell, G. R. and Bolton, M. D., On the micromechanics of crushable aggregates. *Geotechnique*, 1998, **48**, 667–679.
10. Shima, S. and Mimura, K., Densification behaviour of ceramic powder. *Int. J. Mech. Sci.*, 1986, **28**(1), 53–59.
11. Kuhn, L. T., Fleck, N. A. and McMeeking, R. M., Yielding of metal powder bonded by isolated contacts. *J. Mech. Phys. Solids*, 1992, **40**, 1139–1162.
12. Gurson, A. L., A plasticity theory for porous solids. *Int. J. Mech. Sci*, 1972, **14**, 215–224.
13. Akisanya, A. R. and Cocks, A. C. F., Stage I compactions of cylindrical particles under non-hydrostatic loading. *J. Mech. Phys. Solids*, 1995, **43**, 605.
14. Nixon, S.A., Chandler, H.W.On the elasticity and plasticity of dilatant granular materials. *J. Mech. Phys. Solids*, 1999, **47**, 1397–1408.
15. Chandler, H. W., Homogeneous and localised deformation in granular materials: a mechanistic approach. *Int. J. Eng. Sci.*, 1990, **28**, 719–734.
16. Teukolsky, S. A., Press, W. H., Flannery, B. P. and Vetterling, W. T., *Numerical Recipes*. Cambridge University Press, Cambridge, 1986.

17. Song, J. H. and Chandler, H. W., The determination of some compaction properties of ceramic powders using a simple cylindrical apparatus. *Br. Ceram. Trans. J*, 1990, **89**, 49–52.
18. Song, J.H., Compaction of ceramic powders. PhD thesis, University of Newcastle upon Tyne, UK, 1991.
19. Spencer, A.J.M., *Continuum Mechanics*. Longman Scientific and Technical, 1980.
20. Femsys, *FEMSYS User's Manual*, Version 4 edition, 1997.
21. Hibbit, Karlsson and Sorensen. *Abaqus User's Manual*, Version 5.5 edition, 1995.